Surface effects on the photoconducting properties of $SrTiO_3$ thin films

N. Bachi, G. Bridoux, M. Villafuerte, J. M. Ferreyra, J. Kim, C. Figueroa, and S. P. Heluani

Citation: Appl. Phys. Lett. **110**, 091103 (2017); doi: 10.1063/1.4976944
View online: http://dx.doi.org/10.1063/1.4976944
View Table of Contents: http://aip.scitation.org/toc/apl/110/9
Published by the American Institute of Physics

Surface effects on the photoconducting properties of $SrTiO_3$ thin films

N. Bachi,[1] G. Bridoux,[2,a)] M. Villafuerte,[2] J. M. Ferreyra,[1] J. Kim,[3] C. Figueroa,[1] and S. P. Heluani[1]

[1]*Laboratorio de Física del Sólido, Facultad de Ciencias Exactas y Tecnología, Universidad Nacional de Tucumán, 4000 Tucumán, Argentina*

[2]*Consejo Nacional de Investigaciones Científicas y Técnicas - CONICET and Laboratorio de Física del Sólido, Facultad de Ciencias Exactas y Tecnología, Universidad Nacional de Tucumán, 4000 Tucumán, Argentina*

[3]*Neocera LLC., 10000 Virginia Manor Road, Beltsville, Maryland 20705, USA*

(Received 14 October 2016; accepted 7 February 2017; published online 27 February 2017)

We report a study of the photoconducting properties of semiconducting $SrTiO_3$ thin films. The photoconducting spectrum shows a pronounced rise around 3.2 eV with a typical indirect gap dependence, involving a transversal optical phonon of 25 meV. While these features remain unaltered under the influence of an applied electric field in ambient conditions, in a vacuum the rest of the spectrum does not, shifting to lower energies for higher electric fields. Time dependent photoconductivity response while illumination is applied confirms the loss of efficiency of the 3.7 eV transition. At low-temperatures, the photoconducting spectrum at low-electric fields has striking similarities to the ones at room-temperature for high-electric fields. This ability to control the photoconducting response through external parameters is explained considering a model of a downward band bending generated by oxygen vacancies at the surface in concomitant with recent findings at the surface of $SrTiO_3$. *Published by AIP Publishing.*
[http://dx.doi.org/10.1063/1.4976944]

The improvement of the fabrication techniques of transition metal oxide thin films[1] has allowed the emergence of a field of interfaces and surface phenomena.[2] In that regard, $SrTiO_3$ (STO) plays a key role as an ingredient of the most celebrated bilayer in the last few years: $LaAlO_3/SrTiO_3$ in which a downward band-bending at the interface originates a high-mobility 2D electron gas (2DEG).[3,4] On the other hand, recent discoveries have exposed the complex nature at the bare STO surface, which hosts a 2DEG or liquid[5–7] with a delicate interplay of the spin, charge, and orbital degrees of freedom.[8,9]

The properties of this surface can be modified under the exposure of an intense ultraviolet light (UV) of ∼55 eV,[7,10] the presence of adsorbed oxygen,[10] or the generation of oxygen vacancies, V_O;[7,11] the latter are easily produced in STO by a simple thermal annealing in a vacuum[12] and they tend to accumulate on the surface increasing in this way the downward band-bending.[7] At the same time, this simple procedure easily dopes STO with electrons.[12] Since STO has an UV indirect gap of ∼3.2 eV (whose transition involves the creation or destruction of a phonon in order to conserve the momentum)[13] and a direct one of ∼3.7 eV,[14] previous studies have explored the photoconducting properties of bulk crystals resulting in a persistent photoconductivity effect (PPC),[15,16] which is very dependent on the presence of deep-levels inside the gap generated by oxygen vacancies.[15,16] In thin films, it is expected that the surface effects becomes more pronounced and sensitive to external perturbations. In this sense, we have fabricated STO thin films in oxygen deficient conditions with reduced strain[17] and we have been able to tune their photoconducting properties by means of external parameters like excitation voltage, ambient conditions, and temperature.

Homoepitaxial STO thin films were grown by pulsed laser deposition (PLD) on metallic *n*-doped (001) $SrTiO_3$ substrates[12,16,18] at a temperature of 685 °C and a base pressure of 7×10^{-5} Torr (see supplementary material for details). After the fabrication, the film was post-annealed at a temperature of 500 °C and a pressure of 7×10^{-5} Torr during 30 min that is believed that generates a higher concentration of oxygen vacancies at the surface.[12,19–22] The films studied in this work have thicknesses that range between 7 and 9 nm. For the electrical transport measurements, sputtered Au pads (∼10 nm thick and ∼0.2 mm width) were deposited on top of the semiconducting film and on the bottom of the metallic STO substrate, resulting in ohmic contacts.[12,23] The resistances measured on top of the STO thin films have typical values of$\sim 3 \times 10^4 \Omega$. For the same distance between contacts (∼0.3 mm), the corresponding resistance measured on the bottom of the STO substrate is $\sim 1.5 \times 10^3 \Omega$ with a metallic resistive behavior and a negligible photoconducting response. Most of the measurements were performed employing an out of plane configuration (see sketch of Fig. 1(a)) where the metallic STO substrate was used as a bottom electrode. The film was illuminated from top on its whole area (∼10 mm × 10 mm), and the light penetration depth is estimated to be around ∼100 nm for the wavelengths used in this work (see supplementary material for further details).

The photoconducting response of the film when the incident light energy is varied from low to higher values is depicted in Figure 1(a) at room-temperature in air ambient conditions. In this case, a scanning speed of 0.5 nm s^{-1} was used; slower scanning speeds have essentially led to the same overall results. As it can be observed, there is an onset

a)Electronic mail: gbridoux@herrera.unt.edu.ar

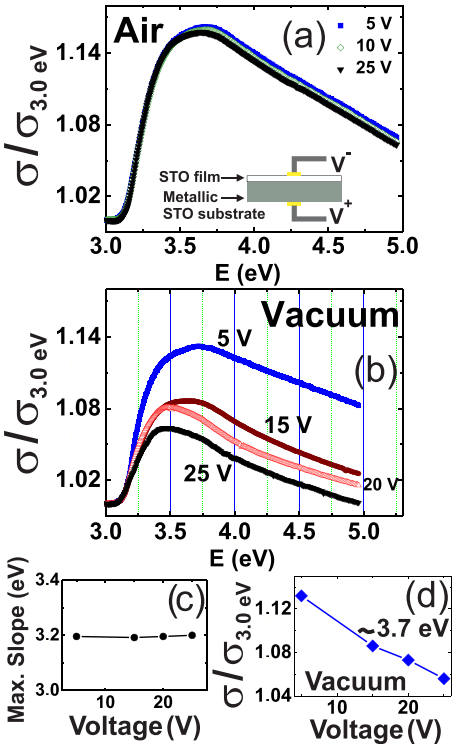

FIG. 1. (a) Conductivity (normalized at its 3.0 eV value) as a function of the incident light energy at room temperature in air ambient conditions. Different scans at different excitation voltages of 5 V (blue squares), 10 V (empty diamonds), and 25 V (black triangles) are shown. The sketch shows the measurement configuration setup. (b) Different scans for different applied voltages of 5 V (blue squares), 15 V (brown circles), 20 V (empty triangles), and 25 V (black triangles) at room-temperature in a vacuum ($\sim 10^{-1}$ Torr). (c) Energy position of the maximum slope for different applied voltages. (d) Conductivity (normalized at its 3.0 eV value) at ~3.7 eV extracted from the spectra of (b) as a function of the applied voltage.

of photoconductivity with a maximum slope at ~3.2 eV, which corresponds to the indirect gap transition of STO.[13] If the energy is further increased, a maximum of conductivity is attained at ~3.7 eV (which coincides with the STO direct transition in these conditions); above this value, photoconductivity starts to decrease due to the fact that at this energy the recombination rate overpasses the generation of photoelectrons to the conduction band (CB). We have measured these photoconductance spectra for different applied excitation voltages; they remain unaltered by their influence. We have repeated these experiments in a vacuum ($\sim 10^{-1}$ Torr), and the results are summarized in Figure 1(b). Remarkably, they show that while the onset and the rise of photoconductivity remain unchanged under the influence of the applied electric field, the rest of the spectrum is very sensitive to it, shifting to lower energies for higher applied voltages. In fact, if the maximum slope of each spectrum is extracted,[24] its position remains at ~3.2 eV independently of the applied electric field (see Fig. 1(c)), which is an indicative that the indirect gap transition is unaffected by this external parameter. At first sight, it can also be noticed that the photoconductivity decreases as the electric field is increased, which is more evident if the normalized conductivity, $\sigma/\sigma_{3.0eV}$, extracted from these spectra at ~3.7 eV is plotted as a function of the applied voltage, see Fig. 1(d).

For a closer examination of photoconductivity, *PC* (defined as $PC = (\sigma - \sigma_{dark})/\sigma_{dark}$), in the range of energies where it is more sensitive to the applied electric field, its time dependent response has been studied when illumination is applied (energy close to ~3.7 eV), and the results are shown in the main panel of Figure 2. At first glance, it can be noticed that after a fast increase in photoconductivity, it slowly tends to saturate reaching a steady state, which is a balance of the photo-generation and recombination processes. In air conditions, *PC* is higher than in a vacuum, while in the latter case, *PC* is lower for higher electric fields, confirming the observations of Figure 1(b). The best fit of our data was attained using the sum of three exponential functions[25] with relaxation times τ_i, where $i = 1$, 2, and 3. Several trial functions like a stretched exponential or a power law did not give satisfactory results. While the fast time responses $\tau_1 \sim 3$ s and $\tau_2 \sim 35$ s are the same for all the curves, the slow time response τ_3 is ~230 s for the curve in air and ~300 s and ~950 s for the curves in a vacuum at 5 V and 25 V, respectively.

In order to explain the photoconducting features exposed in Figs. 1 and 2, we make use of a model where surface effects and band-bending[26] are playing a major role in these films. In this model, oxygen vacancies created during the fabrication of the STO film[12,19–22,27] and the post-annealing generate a positive charge accumulation close to the surface, which results in a downward band-bending in vacuum conditions as it is described in the energy diagram sketch of Fig. 3. Other authors have found that in STO films, minor amounts of Strontium deficiency could drive to an electrical polarization,[28,29] which in turn can build a downward band-bending in vacuum conditions. Using the band-bending expression:[26] $\phi = eN\, e\, d^2/2\varepsilon_r\, \varepsilon_0$, where d is the depletion layer that ranges between 1 and 5 nm,[7,30,31] eN is the effective charge density, ε_r is the relative dielectric constant of STO,[32] and ε_0 is the vacuum permittivity, it is possible to estimate a band-bending energy value of $\phi \simeq 0.5$ eV. In air conditions, the oxygen adsorbed on the surface[33,34] compensates the downward band-bending resulting in an upward band-bending and only a band-to-band transition takes place along the whole thickness of the film (process labeled as 1, see left panel of Fig. 3). In this situation, the application of a high-electric field is somehow blocked by

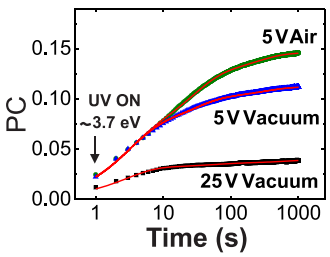

FIG. 2. Evolution of photoconductivity (defined as $PC = (\sigma - \sigma_{dark})/\sigma_{dark}$) as a function of time while an incident light of ~3.7 eV is applied at room-temperature. Experiments under air at 5 V (green circles) and vacuum ($\sim 10^{-1}$ Torr) at 5 V (blue triangles) and 25 V (black squares) were performed. The red lines are the corresponding fittings with the sum of three exponential decaying functions. From these measurements, a voltage-dependent photoconductivity is observed, which is concomitant with the trend noticed in Fig. 1(d) despite those being measured in another film grown in the same conditions.

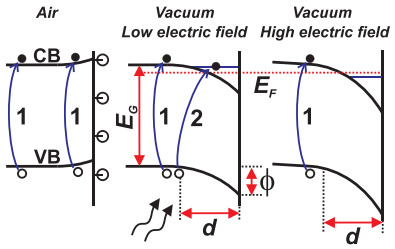

FIG. 3. Sketch of the STO film energy diagram. VB denotes the valence band. In air ambient conditions (left panel), the oxygen adsorbed on the STO surface neutralizes the downward band-bending and the transition takes place between the top of the VB and the bottom of the CB at the energy gap $E_G \sim 3.7$ eV (represented by an arrow and labeled by 1). In a vacuum at low-electric fields (see central panel), the downward band-bending is recovered (in a quantity ϕ) and not only the transition 1 occurs but also a transition (labeled as 2) to a localized level close to the minimum of the CB. At higher electric fields (right panel), the band-bending is increased and this level is covered by the Fermi energy level E_F (represented by a red dashed line) preventing transition 2.

these adsorbed species resulting in an unchanged spectrum, see Fig. 1(a).

In a vacuum at low-electric fields, the scenario is different (see the central panel of Fig. 3); the downward band-bending is recovered, and while away from the surface, process 1 still occurs, in a portion of width d near the surface this process is replaced by a transition to a localized level close to the bottom of the conduction band according to a simple calculation (labeled as process 2). In this calculation, we have numerically evaluated the eigenvalue equation for a triangular potential well (with an infinite barrier on the surface side) of height $\phi \sim 0.5$ eV and width $d \sim 2$ nm. We have obtained a localized state very close to the border of the potential well and another two levels below it. In these conditions, the photo-generation is less efficient than in the former case and consequently it is understandable that the photoconductivity in air at 5 V is higher than the one in a vacuum at the same voltage, in agreement with the time dependent experiment shown in Fig. 2.

On the other hand, if higher electric fields are applied in a vacuum, the downward band-bending becomes more pronounced (see right panel of Fig. 3), and according to our calculations, the mentioned localized level is lowered down enough to be covered by Fermi level energy, E_F. In this situation, it is not possible to promote electrons to this level; process 2 is inhibited in the region of width d and only process 1 takes place at distances higher than d. Moreover, as voltage is increased, this inhibited region for photoconduction of width d grows at the expense of the region where the efficient transition 1 is attained. Hence, it is expected that the overall photoconductivity at high-electric fields (right panel of Fig. 3) becomes lower than the one at low-electric fields in a vacuum (central panel of Fig. 3) where process 2 is still occurring in the region of width d. This is concomitant with the decreased photoconductivity in the former conditions (see Figs. 1(b) and 2) and the shift of the maximum of the spectra (see Fig. 1(b)) to lower energies when the voltage is increased, since this maximum takes place approximately at the energy value above which the recombination process starts to overpass the photo-generation.

If the voltage polarity is reversed, similar results to the ones of Fig. 1 are obtained. In vacuum conditions when the reverse applied bias is increased, the band will eventually bend upward, and the corresponding valence band can confine holes in a region d close to the surface. Then, if illumination is applied, it will not be not so easy to take out electrons from this region and there the transition will be as inefficient as process 2 in the case of the direct polarity.

The photoconducting response at low-temperatures has also been explored. Without illumination, the temperature dependent conductivity measured on top of the film exhibits a typical semiconducting-like behavior, see Fig. 4(a). Above $T \simeq 80$ K, the curve has a metallic temperature dependence that comes from the bottom substrate as we have checked using a parallel resistor network model. At low temperatures, the data were well described by a variable range hopping model (VRH), $\sigma \propto e^{-(T_0/T)^{1/4}}$, where $T_0 \simeq 4 \times 10^3$ K is related to the density of states at the Fermi energy, $N(E_F)$, of shallow levels. It is believed that these shallow levels are related to oxygen vacancies, V_O, which are generated during the fabrication and the post-annealing of the film.[12,16,19–22] Hence, using the relation[35] $N(E_F) = 18/k_B T_0 a_H^3$ with an effective Bohr radius of $a_H \simeq 140$ Å for STO,[36] it gives $N(E_F) \simeq 4.4 \times 10^{19}\,\mathrm{eV^{-1}\,cm^{-3}}$, which is a rather high value for an impurity band considering that for a metallic STO crystal[23] $N(E_F) \simeq 5 \times 10^{20}\,\mathrm{eV^{-1}\,cm^{-3}}$. When illumination is applied, a temperature dependent metallic behavior is attained. This metal-insulator transition (MIT) induced by light has already been reported in bulk STO crystals[16] and it is related to the appearance of an optical phonon below $T \simeq 77$ K,[13,37] which enhances the efficiency of the indirect gap transition. We have also studied the photoconductivity spectrum at low-temperatures ($T = 37$ K), and the results are

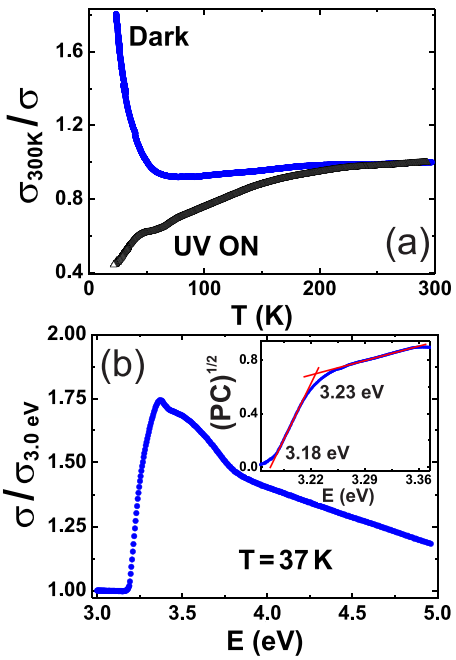

FIG. 4. (a) Temperature dependence of σ_{300K}/σ (where σ_{300K} is the photoconductivity at 300 K) without illumination (blue circles) and under the application of an incident light of ~3.4 eV (empty triangles). (b) Conductivity (normalized at its 3.0 eV value) as a function of the incident light energy at $T = 37$ K. The excitation voltage is 5 V. At the inset, one can notice that the energy dependent photoconductivity, PC, follows a $PC^{1/2}$ behavior in two different regimes that start at ~3.18 eV and ~3.23 eV, respectively. The red lines are guides to the eye.

summarized in Fig. 4(b). Like at room-temperature, the onset of photoconductivity takes place around ∼3.2 eV, but a more detailed analysis is shown in the inset of Fig. 4(b). Considering that the optical absorption coefficient, α, has a $\alpha^{1/2}$ dependence with energy for an indirect transition[24] and assuming that $\alpha \propto PC$ in this range of energies, it is possible to notice that there are actually two regimes that follow a $(PC)^{1/2}$ behavior, one starts at 3.18 eV and the other at 3.23 eV. They correspond to an indirect transition with an indirect gap of 3.20 eV involving the destruction and creation of a 25 meV phonon, respectively. This finding shed light on a large debate about the nature of the phonon that assists the indirect transition in STO at low-temperatures, a 25 meV transverse optical phonon as it was proposed in photoluminescence studies[37] or a 50 meV longitudinal optical one.[13] It is also important to highlight that, in general terms, this low-temperature spectrum at low-excitation voltages is very similar to the ones performed at high-electric fields in a vacuum at room-temperature, see Fig. 1(b). In both spectra, the maximum is shifted to lower energies (it is attained at ∼3.4 eV in the low-temperature one) and a small shoulder appears at ∼3.7 eV when the photoconductivity is already falling, see Figs. 1(b) and 4(b). These striking similarities lead to infer that at low-temperatures the situation is analogous to the one described in the right panel of Fig. 3, that is, at such temperatures, the pressure is very low (around $\sim 10^{-6}$ Torr) and the band-bending will be more pronounced than the one at room-temperature with 5 V and $\sim 10^{-1}$ Torr (see central panel of Fig. 3) and the maximum of the spectrum will be shifted to lower energies like in the high-electric field spectra of Fig. 1(b). The appearance of a maximum at ∼3.4 eV could also be related to a direct transition $X_{5'} \rightarrow X_3$ that was previously observed in STO at low-temperatures in optical absorption experiments.[13]

See supplementary material for thin film fabrication, structural characterization, and photoconductivity measurement details. This work was supported by CIUNT under Grant No. 26/E530, SNMAG, and SINALA facilities.

[1]J. Heber, Nature **459**, 28 (2009).
[2]H. Y. Hwang, Y. Iwasa, M. Kawasaki, B. Keimer, N. Nagaosa, and Y. Tokura, Nat. Mater. **11**, 103 (2012).
[3]A. Ohtomo and H. Y. Hwang, Nature **427**, 423 (2004).
[4]S. Thiel, G. Hammerl, A. Schmehl, C. W. Schneider, and J. Mannhart, Science **313**, 1942 (2006).
[5]A. F. Santander-Syro, O. Copie, T. Kondo, F. Fortuna, S. Pailhès, R. Weht, X. G. Qiu, F. Bertran, A. Nicolaou, A. Taleb-Ibrahimi, P. Le Fèvre, G. Herranz, M. Bibes, N. Reyren, Y. Apertet, P. Lecoeur, A. Barthélémy, and M. J. Rozenberg, Nature **469**, 189 (2011).
[6]N. C. Plumb, M. Salluzzo, E. Razzoli, M. Mansson, M. Falub, J. Krempasky, C. E. Matt, J. Chang, M. Schulte, J. Braun, H. Ebert, J. Minar, B. Delley, K.-J. Zhou, T. Schmitt, M. Shi, J. Mesot, L. Patthey, and M. Radović, Phys. Rev. Lett. **113**, 086801 (2014).
[7]W. Meevasana, P. D. C. King, R. H. He, S-K. Mo, M. Hashimoto, A. Tamai, P. Songsiriritthigul, F. Baumberger, and Z.-X. Shen, Nat. Mater. **10**, 114 (2011).
[8]A. F. Santander-Syro, F. Fortuna, C. Bareille, T. C. Rödel, G. Landolt, N. C. Plumb, J. H. Di, and M. Radović, Nat. Mater. **13**, 1085 (2014).
[9]C. Chen, J. Avila, E. Frantzeskakis, A. Levy, and M. C. Asensio, Nat. Commun. **6**, 8585 (2015).
[10]S. McKeown Walker, A. de la Torre, F. Y. Bruno, A. Tamai, T. K. Kim, M. Hoesch, M. Shi, M. S. Bahramy, P. D. C. King, and F. Baumberger, Phys. Rev. Lett. **113**, 177601 (2014).
[11]R. Di Capua, M. Radovic, G. M. De Luca, I. Maggio-Aprile, F. Miletto Granozio, N. C. Plumb, Z. Ristic, U. Scotti di Uccio, R. Vaglio, and M. Salluzzo, Phys. Rev. B **86**, 155425 (2012).
[12]A. Spinelli, M. A. Torija, C. Liu, C. Jan, and C. Leighton, Phys. Rev. B **81**, 155110 (2010).
[13]M. Capizzi and A. Frova, Phys. Rev. Lett. **25**, 1298 (1970).
[14]P. K. Gogoi and D. Schmidt, Phys. Rev. B **93**, 075204 (2016).
[15]M. C. Tarun, F. A. Selim, and M. D. McCluskey, Phys. Rev. Lett. **111**, 187403 (2013).
[16]G. Bridoux, M. Villafuerte, J. M. Ferreyra, N. Bachi, C. A. Figueroa, and S. P. Heluani, Phys. Rev. B **92**, 155202 (2015).
[17]Z. Huang, Z. Q. Liu, M. Yang, S. W. Zeng, A. Annadi, W. M. Lü, X. L. Tan, P. F. Chen, L. Sun, X. Renshaw Wang, Y. L. Zhao, C. J. Li, J. Zhou, K. Han, W. B. Wu, Y. P. Feng, J. M. D. Coey, T. Venkatesan, and Ariando, Phys. Rev. B **90**, 125156 (2014).
[18]G. Herranz, M. Basletić, O. Copie, M. Bibes, A. N. Khodan, C. Carrétéro, E. Tafra, E. Jacquet, K. Bouzehouane, A. Hamzić, and A. Barthélémy, Appl. Phys. Lett. **94**, 012113 (2009).
[19]A. Ohtomo and H. Y. Hwang, J. Appl. Phys. **102**, 083704 (2007).
[20]J. Shen, H. Lee, R. Valentí, and H. O. Jeschke, Phys. Rev. B **86**, 195119 (2012).
[21]A. R. Silva and G. M. Dalpian, J. Appl. Phys. **115**, 033710 (2014).
[22]W. Sitaputra, N. Sivadas, M. Skowronski, D. Xiao, and R. M. Feenstra, Phys. Rev. B **91**, 205408 (2015).
[23]X. Lin, Z. Zhu, B. Fauqué, and K. Behnia, Phys. Rev. X **3**, 021002 (2013).
[24]A. M. Fox, *Optical Properties of Solids* (Oxford University Press, London, 2010).
[25]S. A. Studenikin, N. Golego, and M. Cocivera, J. Appl. Phys. **83**, 2104 (1998).
[26]Z. Zhang and J. T. Yates, Jr., Chem. Rev. **112**, 5520 (2012).
[27]V. E. Alexandrov, E. A. Kotomin, J. Maier, and R. A. Evarestov, Eur. Phys. J. B **72**, 53 (2009).
[28]H. W. Jang, A. Kumar, S. Denev, M. D. Biegalski, P. Maksymovych, C. W. Bark, C. T. Nelson, C. M. Folkman, S. H. Baek, N. Balke, C. M. Brooks, D. A. Tenne, D. G. Schlom, L. Q. Chen, X. Q. Pan, S. V. Kalinin, V. Gopalan, and C. B. Eom, Phys. Rev. Lett. **104**, 197601 (2010).
[29]J. G. Bednorz and K. A. Müller, Phys. Rev. Lett. **52**, 2289 (1984).
[30]B.-C. Huang, Y.-P. Chiu, P.-C. Huang, W.-C. Wang, V. T. Tra, J.-C. Yang, Q. He, J.-Y. Lin, C.-S. Chang, and Y.-H. Chu, Phys. Rev. Lett. **109**, 246807 (2012).
[31]P. Schütz, F. Pfaff, P. Scheiderer, Y. Z. Chen, N. Pryds, M. Gorgoi, M. Sing, and R. Claessen, Phys. Rev. B **91**, 165118 (2015).
[32]E. A. Geiss, R. L. Sandstrom, W. J. Gallagher, A. Gupta, S. L. Shinde, R. F. Cook, E. I. Cooper, E. J. M. O'Sullivan, J. M. Roldan, A. P. Segmuller, and J. Angilello, IBM J. Res. Dev. **34**, 916 (1990).
[33]E. G. Barbagiovanni, V. Strano, G. Franz, and S. Mirabella, Appl. Phys. Lett. **109**, 143104 (2016).
[34]V. Vonk, S. Konings, G. J. Van Hummel, S. Harkema, and H. Graafsma, Surf. Sci. **595**, 183 (2005).
[35]N. Mott and E. Davis, *Electronic Processes in Non-Crystalline Materials*, 2nd ed. (University Press, Oxford, 1979).
[36]P. P. Edwards and M. J. Sienko, Phys. Rev. B **17**, 2575 (1978).
[37]Y. Yamada and Y. Kanemitsu, Phys. Rev. B **82**, 121103(R) (2010).